Received 9 October 2023; revised 28 November 2023; accepted 7 December 2023. Date of publication 13 December 2023; date of current version 30 January 2024.

Digital Object Identifier 10.1109/OJAP.2023.3341638

Linearly Scanning Spoof Surface Plasmon Polaritons Leaky-Wave Antenna With High Scanning Rate

YUE WANG[1], SHENGYING LIU[2], CHUNSHENG GUAN[3], HAO YU[4], JINXIANG WANG[1], QUN WU[1] (Senior Member, IEEE), CHANGFEI ZHOU[5], AND XUMIN DING[6] (Member, IEEE)

[1]Microelectronics Center, Harbin Institute of Technology, Harbin 150001, China
[2]Department of Antenna Technology, Beijing Institute of Remote Sensing Equipment, Beijing 100854, China
[3]Air and Missile Defense College, Air Force Engineering University, Xi'an 710051, China
[4]Beijing Institute of Electronic System Engineering, Beijing 100854, China
[5]School of Information and Communication Engineering, Dalian University of Technology, Dalian 116024, China
[6]School of Instrumentation Science and Engineering, Harbin Institute of Technology, Harbin 150080, China

CORRESPONDING AUTHORS: C. GUAN AND X. DING (e-mail: chunshengguan@163.com; xuminding@hit.edu.cn)

This work was supported in part by the National Natural Science Foundation of China under Grant 62275063 and Grant 62171153, and in part by the Natural Science Foundation of Heilongjiang Province under Grant YQ2021F004.

ABSTRACT In this paper, a wide-angle linearly scanning leaky-wave antenna (LWA) based on spoof surface plasmon polaritons (SSPPs) with a very high scanning rate is proposed. A sine curve period is introduced to construct the SSPPs transmission line in the form of a sine curve, which can transform the dispersion curve to the fast wave region to realize the desired dispersion properties for linearly high scanning rate LWA. The simulated results show that the proposed LWA achieves a scanning angle range of 109° over a narrow operation bandwidth of 7.73–8.13 GHz, implying high linearity, and a high scanning rate. A prototype is fabricated and measured, indicating that the measured scanning angle range is 100° within the frequency band of 7.82–8.21 GHz, and the relative average scanning rate (RASR) is 2053.4°. Compared with ideal linear scanning in the operating frequency band, the mean absolute value error (MAVE) of the measured scanning angle-frequency curve is 1.032°, which validates the proposed design with good agreement between the simulated and measured results. The high scanning rate and scanning linearity performances of the LWAs exhibit great value in reducing both the occupation of electromagnetic spectrum resources and the requirements of accuracy for transmitters and receivers, respectively.

INDEX TERMS Leaky-wave antenna (LWA), high scanning rate, linear scanning, spoof surface plasmon polaritons (SSPPs).

I. INTRODUCTION

THE LEAKY wave antenna is a guided wave structure that continuously couples electromagnetic waves to space along the transmission line, for which the radiation direction is determined by the phase propagation constant on the transmission line and period of periodic antenna structure [1], [2]. LWAs are widely used in radar and communication systems due to their advantages of beam scanning without the need of mechanical scanning, as well as the performances of low cost and high gain [3], [4], [5], [6], [7], [8]. High scanning rate LWAs have tremendous advantages in radar and electromagnetic imaging, reducing the bandwidth requirements of digital-to-analog converters and baseband signal processing systems [9], [10], [11], [12]. LWAs can be divided into two categories, which are fast wave antennas and slow wave antennas [13], [14], [15], [16]. For fast wave antennas, the phase propagation constant is smaller than the wave number k_0 of the free space, which means it can radiate energy into free space as the wave travels faster than the wave speed in free space. Since the phase propagation constant is greater than 0, fast wave antennas can only radiate forward. The phase propagation constant of the slow wave antenna

is larger than k_0, for which the periodic structure is needed to generate the higher harmonics appearing in the fast wave region.

There are three general methods to achieve periodic LWA of planar structures. One method is to utilize periodic structures on the transmission line itself [9], [17], [18], [19], [20], [21], [22], such as SSPPs LWAs with periodic impedance modulation [23], SSPPs LWAs that utilize their own periodicity [24], and metagrating [25], [26], [27]. However, the periodic structure itself can affect the transmission line's dispersion curve, increasing the difficulty of adjustment. The second method is to load periodic patches around the transmission line or periodically open gaps on the transmission line [18], [28], [29], [30], [31], [32]. This does not affect the dispersion curve of the transmission line, but the size of the patches or gaps limits the minimum period of the LWA. The third method is to periodically bend the transmission line, such as the Goubau line LWAs with periodic bending [33], [34] and the SSPPs LWAs with periodic bending [35]. This simple structure avoids affecting the dispersion curve of the transmission line and achieves small periods, increasing the adjustment range of the periodic LWAs.

In wireless systems with the requirement of beam scanning, the scanning rate of a LWA is an important evaluation metric [36]. An LWA with a high scanning rate can achieve a large angle beam scanning in a narrow frequency band, reducing the band occupation and transceiver requirements while maintaining the device's performance. In recent years, related researchers have conducted in-depth research on high scanning rate LWAs [9], [10], [11], [12], [36], [37], [38], [39], [40], [41], [42], which not only greatly improve the scanning rate of LWAs, but also realize circularly polarized [39], [43], dual-beam [12], wide-angle [9], [11], [38], [42], gain-stabilized high scanning rate LWAs [38], etc. Also, the scanning linearity of the LWA is another important index to evaluate the antenna performance. With linear scanning, the scanning beam of the antenna varies uniformly when the operating frequency changes, reducing the accuracy requirements of radar and communication systems. To the best knowledge of the author, only one paper combined these two indexes to achieve a linear scanning of 6.7°- 67.5° operating from 11.1 to 12.1 GHz [36], but it has a high profile and can only radiate forward because it is a fast wave waveguide LWA.

In this paper, a SSPPs LWA with sine period-bending is proposed to implement wide-angle linear scanning and a high scanning rate. The dispersion curves for the linear scanning and high scanning rate leaky antenna are investigated. SSPPs structure is used to manipulate the dispersion characteristic of the transmission line, and the sine period-bending structure makes it coincide with the desired dispersion curves of the designed LWA. Measurement results show that the proposed antenna achieves a linear scanning of 100 ° and a high scanning rate within 7.82-8.21 GHz. This antenna shows important applications in reducing the bandwidth and equipment accuracy requirements of radar and communication systems.

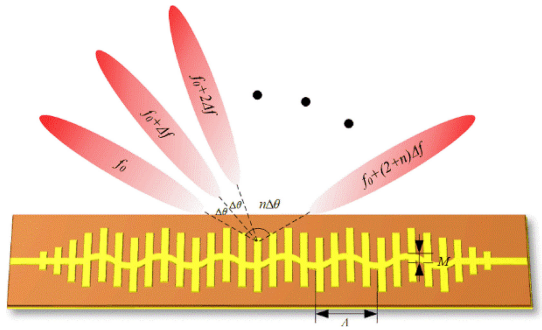

FIGURE 1. Schematic of the proposed LWA with high scanning rate and linear scanning performances.

II. PRINCIPLE AND ANALYSIS

Fig. 1 shows the schematic of the proposed LWA with a high scanning rate and linear scanning performance. The transmission line is bent along the sine curve (1) to transform the equivalent propagation constant into the radiation region and the nth-order equivalent propagation is shown in (2) [36]. A high scanning rate means the beam can cover a wide range within a narrow operational frequency band, while linear beam scanning property means the scanning angle varies with frequency uniformly. To achieve these desired functions, the dispersion curve of the LWA is studied, which determines the beam scanning characteristics of the LWA [36].

$$O(x) = M\,sin(2\pi/\Lambda x) \tag{1}$$

where M is the amplitude of the sine function, and Λ is the period.

$$\beta_n = \beta_{unit} + 2\pi n/\Lambda \tag{2}$$

where β_n is the equivalent propagation constant of the *nth* order and β_{unit} is the transmission line propagation constant.

A. PRINCIPLE OF LINEAR SCANNING

The relationship between the operating frequency of the LWA and the radiation angle for linear beam scanning performance can be described as:

$$\theta = af + b \tag{3}$$

where f is the operating frequency, θ is the angle between the beam direction and the normal of the antenna surface, a and b are arbitrary constants. As shown in (4), the radiation angle is determined by the propagation constant of the LWA [36]:

$$\sin(\theta) = \frac{\beta}{k_0} \tag{4}$$

where β is the propagation constant and k_0 is the wave number in free space. According to (3) and (4), the relation between desired dispersion curves and constants a and b can be obtained, as shown in (5):

$$\beta = \frac{2\pi}{c} \cdot f \cdot \sin(af + b) \tag{5}$$

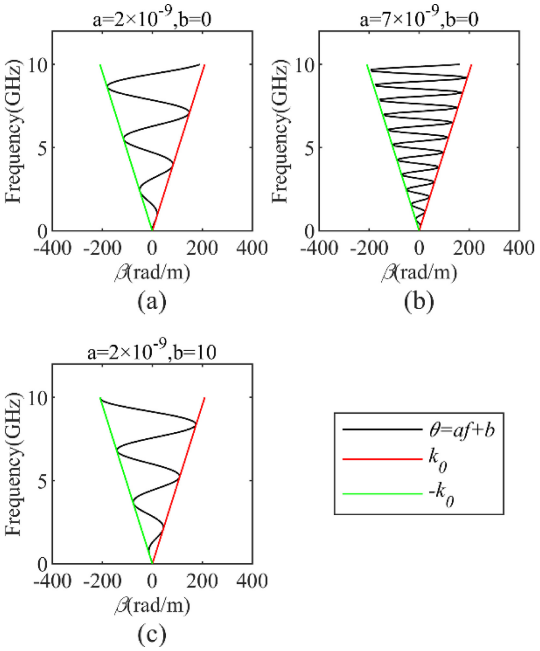

FIGURE 2. Dispersion curves of linear scanning LWA with variables of (a) a = 2×10^{-9}, b = 0, (b) a = 7×10^{-9}, b = 0, and (c) a = 2×10^{-9}, b = 10.

Linear dispersion curve with a low slope in the fast wave region can achieve linear beam scanning performance. Fig. 2 shows the typical dispersion curves with different a and b according to (5). The red and green lines are k_0 and $-k_0$, which represent radiation angles of 180 ° and −180 °, respectively. The black lines are the dispersion curves of linear beam scanning as we proposed. Any section of the black line starting with the green line and ending with the red line represents a scanning range of −180 ° to 180 °. According to Fig. 2 (a) and (b), the constant a only affects the slope of the dispersion curve, and the dispersion curve can be regarded as a straight line in the region from $-k_0$ to k_0 as a increasing. On the contrary, the constant b only changes the initial phase of the dispersion curves, without any effect on the slope. In other words, the β can almost all overlap with any linear dispersion curve with a low slope when a is large enough and b is suitable.

B. PRINCIPLE OF HIGH SCANNING RATE PERFORMANCE

The scanning rate describes the speed of beam scanning with the change of frequency, which can be quantitatively analyzed by the relative average scanning rate (RASR), as shown in (6) [36].

$$S_{RASR} = \frac{\Delta\theta}{\Delta f / f_c} \tag{6}$$

here $\Delta\theta$ (Deg.) is the beam scanning range, Δf is the scanning frequency bandwidth and f_c is the center frequency. To investigate the relationship between scanning rate and linear scanning, equation (3) is substituted into (6), as shown

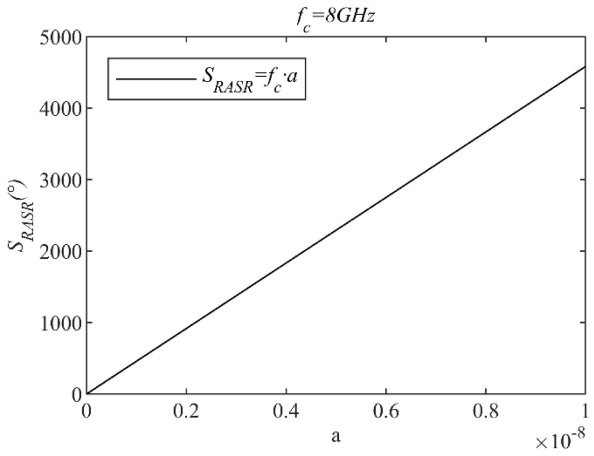

FIGURE 3. The value of RASR(Deg.) with different *a*.

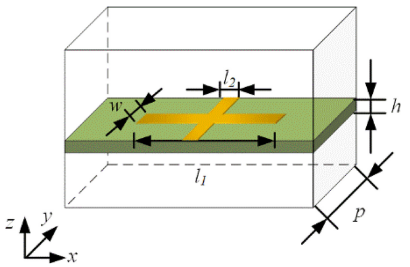

FIGURE 4. SSPPs unit cell.

in (7), from which we can find that the RASR is only affected by a with a constant coefficient f_c:

$$S_{RASR}(rad) = f_c \cdot a \tag{7}$$

Fig. 3 shows the RASR with different a with center frequency of 8 GHz. As we discussed, a high scanning rate and high scanning linearity can be achieved with a large value of a in (3).

III. DESIGN AND ANALYSIS OF THE PROPOSED LWA

To achieve a LWA with a high scanning rate and scanning linearity, the dispersion curve of the open transmission line needs to be designed with a low slope. Then, its equivalent dispersion curve can be overlapped with the desired dispersion curve in the fast wave region by introducing period structure. SSPPs are utilized here to realize the desired open transmission line. Fig. 4 shows the proposed SSPPs unit cell structure, which is composed of a perfect electric conductor (PEC) ground, a lossless dielectric substrate with a relative permittivity of 2.2, and a cross-shaped PEC patch on the top. Here p is the period, and h is the thickness of the unit cell, l_1, l_2, w are the parameters of the cross-shaped patch. To analyze the electromagnetic characteristics of the proposed unit, the commercial electromagnetic simulation software CST Microwave Studio is used to simulate the dispersion curve. With an air box that has a thickness of 60 mm placed on the unit cell, the boundaries along the x

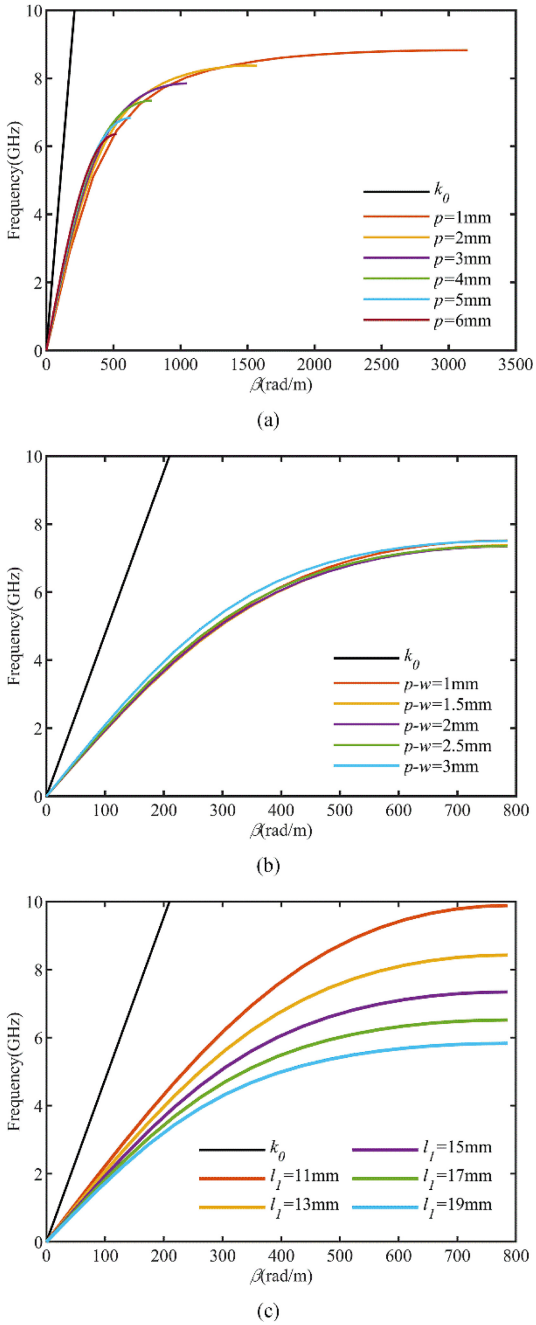

FIGURE 5. Dispersion curves with different (a) period p, (b) gap width p-w, and (c) metal strip length l_1, respectively.

and y axes are set to be periodic and the boundary along the z axis is electric ($E_t = 0$).

Fig. 5 shows the dispersion curves with different parameters. Fig. 5 (a) shows the effect of period p on the dispersion curve while w/p keeps to be a constant. The cutoff frequency and the maximum propagation constant increase as p decreases. So a long enough dispersion curve with a low slope can be obtained with a smaller value of p to overlap the desired dispersion curve. Fig. 5 (b) shows the effect of the gap width (p-w) between two branches while p keeps to be 4 mm. It can be seen that the gap width has almost

TABLE 1. Parameters of LWA unit cell structure.

Parameters	p	h	l_1	l_2	w
Values(mm)	2	0.787	15	1	2.3

no impact on the dispersion curve of the unit cell. Fig. 5 (c) shows the effect of length l_1 on the dispersion curve while p and w are set to be 4 mm and 2 mm, respectively. It illustrates that the cutoff frequency of the dispersion curve becomes smaller and the slope becomes more uniform with a smaller slope change at the end range as l_1 increases, which can overlap with the desired dispersion curve better. So by optimizing two parameters p and l_1, the desired dispersion curve can be realized.

To obtain a quasi-linear dispersion curve segment with a low slope, p and l_1 are optimized to be $w = 0.5p$, and the optimized parameters are shown in Table 1. Then, to make the dispersion curve of the -1st order coincide with that of (3), the modulation period Λ, a, and b are optimized at the same time.

The optimization process of antenna parameters is as follows:

1. Determine the a of the antenna in (3) as required. According to (7), a can be determined according to the required scanning rate and operating frequency. Take any value b and plot the ideal linear scanning dispersion curve as shown by the black line in Fig. 6.
2. Change the period p of the unit and the length l_1 of the branch to simulate the dispersion curve β_{unit} of the unit. Then the transmission line formed by this unit is bent along the sine curve of period Λ, and the equivalent transmission constant obtained is $\beta_{unit} - 2\pi/\Lambda$, as shown in the purple curve in Fig. 6.
3. Adjust b and Λ so that the purple and black lines coincide. If it does not coincide, go back to step 2 and change the values of l_1 and p until the purple and black lines coincide.

Fig. 6 shows the ideal -1st order dispersion curve and beam directions of the optimized linear scanning SSPPs LWA with $a = 4.333 \times 10^{-9}$, b = 3.0291, and modulation period $\Lambda = 6.5$ mm. The purple line in Fig. 6 (a) is the -1st order dispersion curve of the optimized unit cell after bending along $M\sin(\Lambda x)$. According to [35], when almost all of the energy is radiated out, M has little effect on the gain of the antenna. Through simulation, it is verified that when $M = 0.4$, almost all the energy of the antenna can be radiated out. The lower right corner is a local zoomed-in view, and it can be seen that in the fast wave region, the purple and black lines almost completely overlapped, indicating that it can achieve linear scanning over a large scanning range. The slope of the purple line is very large in radiation range, which can achieve a high scanning rate. The red and black lines in Fig. 6 (b) are the relationships between the scanning angle and operating frequency for the ideal and the modulated unit, respectively, corresponding to the black and purple lines in

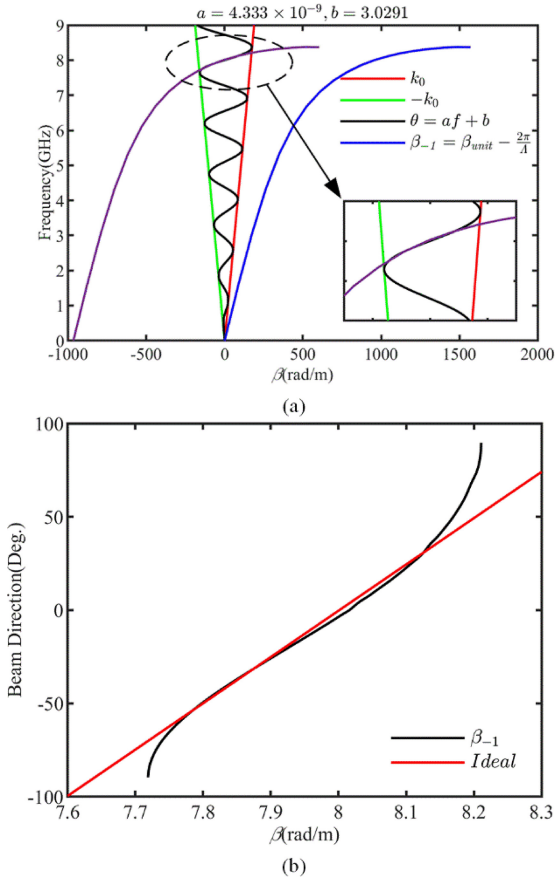

FIGURE 6. The ideal −1st order (a) dispersion curve and (b) beam directions of optimized linear scanning SSPPs LWA.

Fig. 6 (a). It can be found that theoretically a quasi-linear scanning of 100 ° from 7.75 to 8.15 GHz can be achieved.

IV. SIMULATION AND EXPERIMENTAL RESULTS

To verify its performance, the proposed antenna prototype is simulated, fabricated, and measured. The feeding structure and the radiation performance of the proposed antenna and the effect of material loss are discussed in turn.

A. DESIGN OF FEEDING STRUCTURE

Firstly, a tapering SSPPs transmission line is designed to match the antenna to a 50 Ω microstrip line, as shown in Fig. 7 (a). The width of the microstrip line is 2.3 mm with the characteristic impedance of 50 Ω, which is the same with the width of the connecting line in the center of the SSPPs unit. The tapering transmission line is composed of 18 SSPPs units with successively narrower widths, and the width difference of adjacent individual cells keeps the same value of dl. The terminal is a microstrip line of length l_c connected to the SMA port. To verify the performance of the matching lines, the ends of SSPPs transmission lines with the length of l_s are connected to the microstrip lines using the designed matching lines. The parameters of the overall structure are shown in Table 2. The substrate of the overall

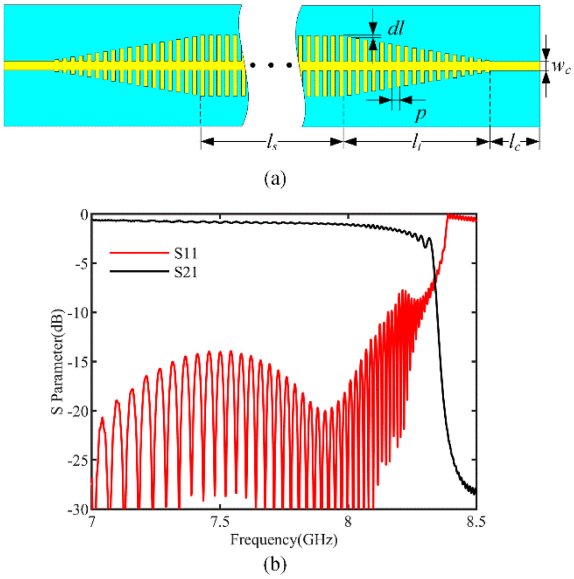

FIGURE 7. (a) Configuration and (b) simulated S Parameters of SSPPs transmission line with gradual matching line.

TABLE 2. Parameters of SSPPs transmission line.

Parameters	p	dl	l_s	l_l	l_c	w_c
Values(mm)	2	0.787	208	36	10	2.3

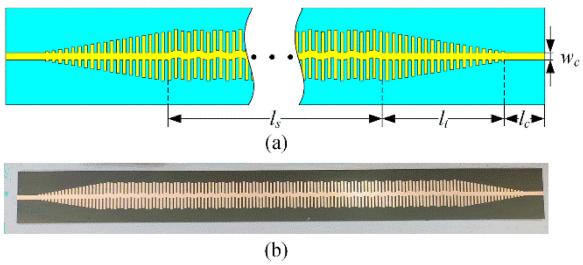

FIGURE 8. (a) Configuration and (b) fabricated prototype of proposed LWA based on period modulation.

structure remains the same. Fig. 7 (b) shows the simulated S parameters of the transmission line, a significant cutoff frequency, and very low insertion loss are verified, proving the excellent performance of the designed feeding structure.

B. DESIGN AND SIMULATION OF THE PROPOSED LWA

Fig. 8 shows the configuration and fabricated prototype of the proposed LWA based on spatial phase modulation. As shown in Fig. 8 (a), the propagation constant of the transmission line can be shifted to −1 order by bending the transmission line periodically. The implementation method is to bend the narrow central connecting line of SSPPs according to the sine function $M\sin(\Lambda x)$. The long branches float up and down with the narrow central line, which keeps at the midpoint of the branch. After optimization, M is taken as 0.4, and Λ is 6.5 mm as discussed in Section III. Fig. 8 (b) shows the prototype fabricated utilizing Rogers 5880 of which the copper thickness is 9 μm, surface roughness is

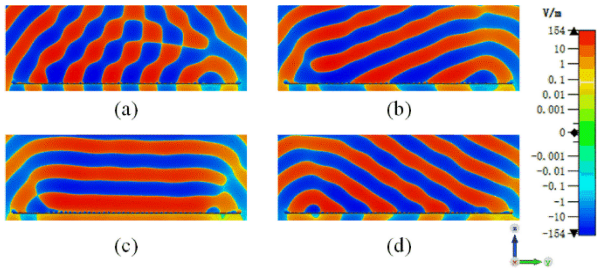

FIGURE 9. The simulated radiation electric field E_x of the proposed LWA at (a) 7.9 GHz, (b) 8.0 GHz, (c) 8.1 GHz, (d) 8.2 GHz, respectively.

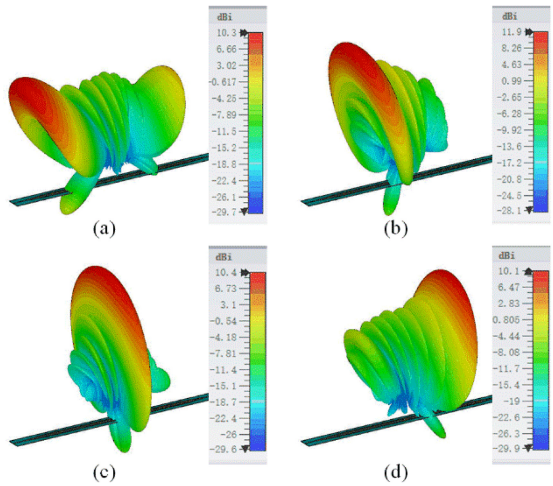

FIGURE 10. Simulated radiation patterns of the proposed LWA at (a) 7.9 GHz, (b) 8.0 GHz, (c) 8.1 GHz, and (d) 8.2 GHz, respectively.

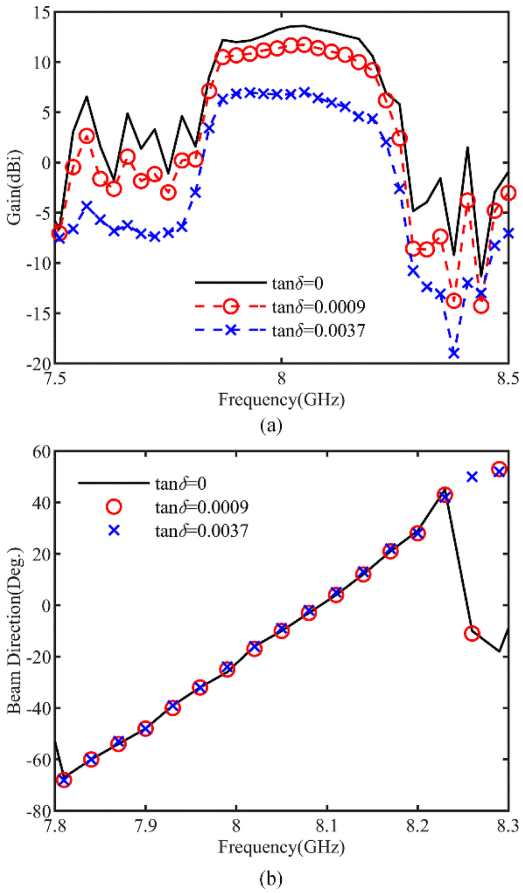

FIGURE 11. Simulated (a) radiation gain and (b) beam direction with different dielectric loss tangents (tanδ).

about 1.3 μm and relative dielectric constant is 2.2 with a loss tangent of 0.0009.

To verify its performance, the proposed antenna is simulated with lossless material and PEC. Fig. 9 and Fig. 10 present simulated electric field distributions and radiation patterns at four operating frequencies, respectively. The wavefront distribution of the radiation electric field at each frequency point is very uniform. The performance of the radiation pattern also agrees very well with the theoretical prediction in Section III.

C. INFLUENCE OF THE DIELECTRIC LOSS TANGENT OF THE SUBSTRATE

In fact, the antenna is fabricated using lossy materials, so it is necessary to analyze the influence of dielectric loss on the antenna performance. Fig. 11 shows the effect of dielectric loss on directionality and gain. Firstly, the antenna is simulated when the metal is PEC and the roughness of surface is 0. The loss tangents of two common dielectric substrates (Rogers 5880 of 0.0009 and Rogers 4350B of 0.0037) are chosen for comparison with lossless material. It can be seen that when the loss tangent increases, the gains of the antenna decrease in the whole operational bandwidth, but the radiation directions remain almost the same with good linearity and a high scanning rate. For the proposed SSPPs LWA, when the frequency is beyond 8.25 GHz, the phase propagation constant is larger than k_0 and there will be no obvious radiation main lobe, as shown that larger errors occur at high frequencies.

D. INFLUENCE OF METAL CONDUCTIVITY AND SURFACE ROUGHNESS

Fig. 12 shows the effect of metal loss and surface roughness. The LWA is simulated when the patch is made of PEC and the copper with four surface roughness is chosen for comparison. Typical roughness values of rolled copper, electrodeposited copper with thicknesses of 9μm and 18μm of Rogers 5880 are utilized here as 0.4μm, 1.3μm and 2.0μm, respectively, which are offered by ROGERS CORPORATION [44]. It can be seen that the gains of the antenna decrease, and the radiation direction shifts as the decrease of metal conductivity and the increase of surface roughness. However, the scanning linearity and the high scanning rate can remain satisfactory.

The decrease of the gain is mainly due to the structure. Because near the cutoff frequency, the propagation constant (real part of the k-vector) of SSPPs is so large that the field is spatially squeezed, leading to strong absorption [45]. According to the above simulation results, the source of high

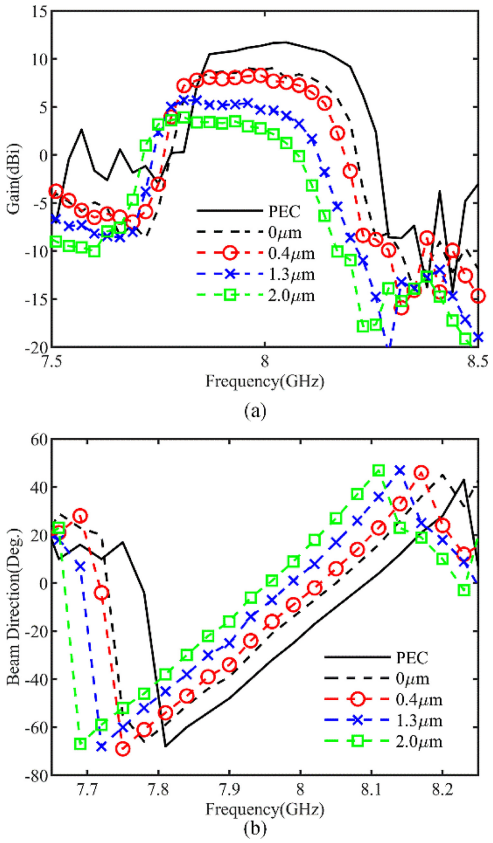

FIGURE 12. Simulated (a) radiation gain and (b) beam direction with PEC and copper with different surface roughness.

FIGURE 13. Schematic diagram of the measurement setup.

loss is mainly the dielectric loss and the surface roughness of the metal, rather than the main source of the usual thought is only the dielectric loss. Therefore, the high-frequency circuit board with a lower dielectric constant and lower surface roughness can improve the gain.

E. SIMULATION AND MEASUREMENT

To obtain the performance of the prototype, the near-field measurement system is used to measure the S parameter and radiation patterns. As shown in Fig. 13, the antenna is surrounded by a ring-shaped housing, in which many pyramidal absorbers and dual-polarized microwave probes are

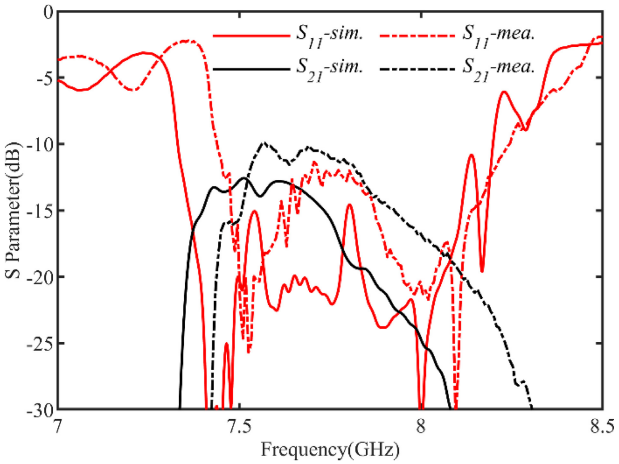

FIGURE 14. Simulated and measured S parameters of the prototype.

evenly distributed to measure the electric field distribution in a plane.

The platform on which the antenna is located can be rotated horizontally by 360 ° to obtain the electric field distribution on a spherical surface surrounding the antenna. The entire measurement system is housed in a metal cabinet with absorbers inside. The vector network analyzer is connected to this measurement system to provide S-parameters. A computer is connected to both the measurement system and the vector network analyzer to provide control and data post-processing. The three-dimensional radiation direction pattern can be obtained using the near-field to far-field algorithm provided by the measurement system of SATIMO. The main polarization and cross-polarization of the antenna are measured together.

To make the simulation closer to the real application scenario, the material parameters of Rogers5880 with a relative dielectric constant of 2.2, a loss tangent of 0.009, copper, and surface roughness of 1.3μm are used for simulation.

Fig. 14 shows the simulated and measured S parameters of the prototype. The overall trend of S parameters is consistent, and the measured results only have a very narrow frequency offset. This may be caused by errors between the relative dielectric constant of the substrate and the nominal value, as well as errors in fabrication, since the antenna proposed is very sensitive to material parameters as we discussed above.

Fig. 15 shows the simulated and measured normalized radiation patterns of the prototype. The simulated results show that the proposed LWA achieves a scanning angle range of 109 ° over a narrow operation bandwidth of 7.73–8.13 GHz, implying a high scanning rate and scanning linearity. The measured scanning angle range is 100 ° in the frequency band of 7.82–8.21 GHz, and the relative average scanning rate is 2053.4 °. Although there is an offset of about 0.1 GHz between the simulation and measured results, both the simulation and measured results maintain good scanning linearity and high scanning rate.

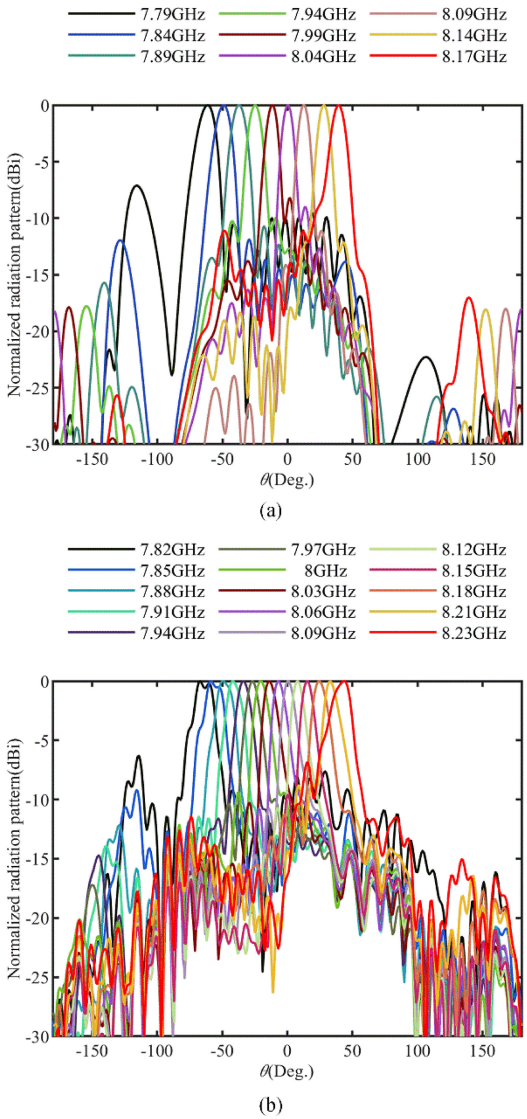

FIGURE 15. (a) Simulated and (b) measured normalized radiation patterns of the prototype.

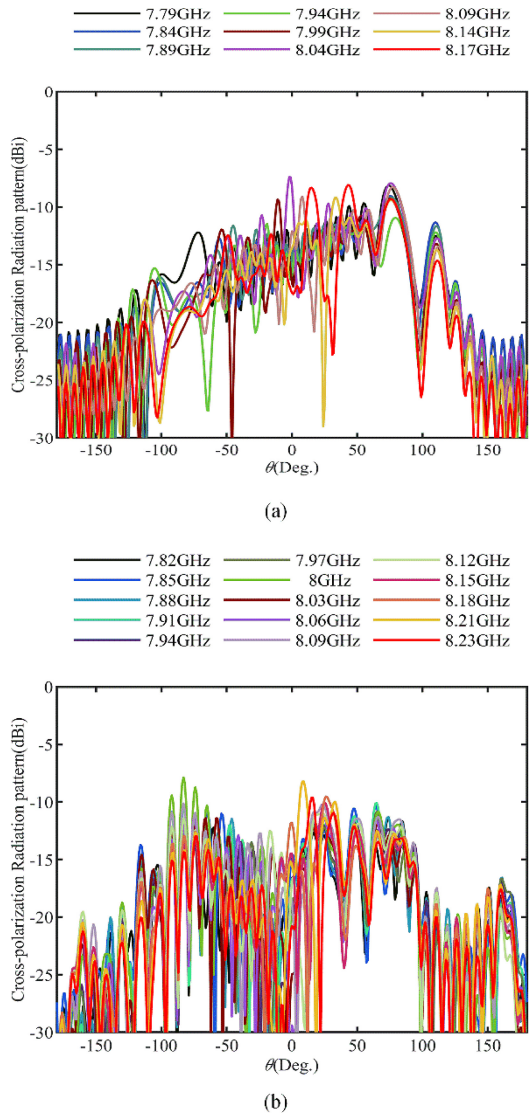

FIGURE 16. (a) Simulated and (b) measured cross-polarization radiation patterns of the prototype.

Fig. 16 shows the cross-polarized radiation pattern of simulation and measurement. At the operating frequency, the cross-polarized radiation energy is very low and has little effect on the radiation characteristics.

Fig. 17 shows the simulated and measured radiation gain and beam direction of the prototype. There is a shift of about 0.1 GHz between the simulated and measured gains, which is consistent with the S parameter results, but the overall trend remains the same. The gain error of 1 dB is caused by a fabricated error as shown in Fig. 17 (a). The radiation pattern and gain trend of the antenna in the measurement and simulation results are basically consistent after correction, as shown in Fig. 17 (a). The reason of 1dB loss in the gain maybe machining errors, SMA adapter losses, and material errors. Fig. 17 (b) shows the simulated and measured beam radiation direction.

The solid black line is the ideal beam scanning curve for our design, as shown in Fig. 17. The red circle line is the simulated beam scanning curve, which is very close to the ideal value, proving the correctness of the proposed theory. The blue cross line is the scanning curve of the measured beam, which deviates from the design value by about 0.1 GHz. To better evaluate the scanning linearity of the measured results, the solid black line has been shifted horizontally by about 0.1 GHz to become the dashed black line, keeping the slope constant and making it as close to the blue line as possible. It can be found that the scanning linearity of the measurement results shows good agreement with the theoretical design.

To evaluate the scanning linearity, the mean absolute value error (MAVE) is used to calculate the error between the measured and ideal results as in (8):

$$MAVE = 1/N \sum_{i=1}^{N} |\theta_i - T_i| \tag{8}$$

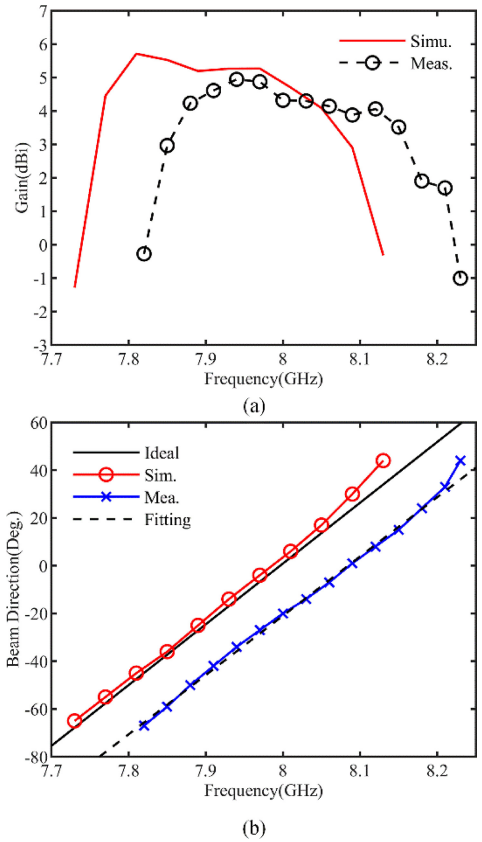

FIGURE 17. Simulated and measured (a) radiation gain and (b) beam direction of the prototype.

TABLE 3. Comparison of different high RASR antennas and linear antennas.

Reported Works	Center Frequency (GHz)	Scanning Range (deg)	RASR (deg)	Gain (dBi)	Linearity (deg)
[11]	9.6	152	660.9	>9	-
[36]	11.5	40.8	589.3	15.2-18	1.488
[40]	2.5	27	337.5	<8	-
[42]	13.7	35	1198.8	>9.2	-
[46]	11.1	123	1365.3	7.3-9.6	-
This Work	8.015	100	2053.4	<5	1.032

here N is the number of measured points of radiation patterns, θ_i and T_i are ith measured and ideal points of radiation pattern, respectively. The *MAVE* of the results in Fig. 17 (b) is 1.032.

To prove the advantages of our design, the results of previously reported LWAs in Table 3 are listed for comparison. Few works consider the scanning linearity of LWAs except [36]. The RASR of our design is the largest compared to other published LWAs, meanwhile, the best scanning linearity with a large scanning range can be achieved. The gain of our proposed work can be further improved by utilizing metals with lower electrical conductivity, like gold and silver, and metals with lower surface roughness.

V. CONCLUSION

A SSPPs LWA with a high scanning rate and linear scanning is proposed. Dispersion properties of linear high scanning rate LWA are studied in fast wave regions. The measured scanning angle range is 100 ° in the frequency band of 7.82–8.21 GHz, and the RASR is 2053.4 °. The MAVE of the measured scanning angle-frequency curve is 1.032 °, showing good linearity as designed. This antenna may find application potential in reducing the accuracy and bandwidth requirements of A/D converters in radar systems.

REFERENCES

[1] R. Honey, "A flush-mounted leaky-wave antenna with predictable patterns," *IRE Trans. Antennas Propag.*, vol. 7, no. 4, pp. 320–329, Oct. 1959, doi: 10.1109/TAP.1959.1144703.

[2] E. A. F. Abdallah, A. A. Mitkees, S. A. Hamdy, and A. A. Elsohly, "Propagation constant of microstrip leaky-wave antennas," *Microw. Opt. Technol. Lett.*, vol. 3, no. 12, pp. 435–439, 1990, doi: 10.1002/mop.4650031210.

[3] M. Alibakhshikenari, B. S. Virdee, A. Ali, and E. Limiti, "A novel monofilar-Archimedean metamaterial inspired leaky-wave antenna for scanning application for passive radar systems," *Microw. Opt. Technol. Lett.*, vol. 60, no. 8, pp. 2055–2060, 2018, doi: 10.1002/mop.31300.

[4] Y. Cao and S. Yan, "Multi-beam SIW leaky-wave antenna with 2-D beam scanning capability for millimeter-wave radar applications," *Int. J. RF Microw. Comput.-Aided Eng.*, vol. 31, no. 5, May 2021, Art. no. e22600, doi: 10.1002/mmce.22600.

[5] H. Matsumoto, I. Watanabe, A. Kasamatsu, and Y. Monnai, "Integrated terahertz radar based on leaky-wave coherence tomography," *Nat. Electron.*, vol. 3, no. 2, pp. 122–129, Feb. 2020, doi: 10.1038/s41928-019-0357-4.

[6] P. Hudec, P. Panek, and V. Jenik, "Multimode adaptable microwave radar sensor based on leaky-wave antennas," *IEEE Trans. Microw. Theory Tech.*, vol. 65, no. 9, pp. 3464–3473, Sep. 2017, doi: 10.1109/TMTT.2017.2653104.

[7] V. Ebrahimi, L. Yousefi, and M. Mohammad-Taheri, "Enabling inter- and intra-chip optical wireless interconnect by the aid of hybrid plasmonic leaky-wave optical antennas," *Opt. Commun.*, vol. 382, pp. 119–126, Jan. 2017, doi: 10.1016/j.optcom.2016.07.037.

[8] C. DiNallo, F. Frezza, A. Galli, G. Gerosa, and P. Lampariello, "Stepped leaky-wave antennas for microwave and millimeter wave applications," *Ann. Telecommun.*, vol. 52, nos. 3–4, pp. 202–208, Mar. 1997.

[9] G. Zhang, Q. Zhang, Y. Chen, and R. D. Murch, "High-scanning-rate and wide-angle leaky-wave antennas based on glide-symmetry goubau line," *IEEE Trans. Antennas Propag.*, vol. 68, no. 4, pp. 2531–2540, Apr. 2020, doi: 10.1109/TAP.2019.2951524.

[10] D. Ma et al., "Single-shot frequency-diverse near-field imaging using high-scanning-rate leaky-wave antenna," *IEEE Trans. Microw. Theory Tech.*, vol. 69, no. 7, pp. 3399–3412, Jul. 2021, doi: 10.1109/TMTT.2021.3065713.

[11] L. Jidi, X. Cao, J. Gao, T. Li, H. Yang, and S. Li, "Ultrawide-angle and high-scanning-rate leaky wave antenna based on spoof surface plasmon polaritons," *IEEE Trans. Antennas Propag.*, vol. 70, no. 3, pp. 2312–2317, Mar. 2022, doi: 10.1109/TAP.2021.3111182.

[12] Z. Peng, W. Yang, S. Shi, M. Jiang, J. Gao, and G. Zhai, "High scanning rate asymmetrical dual-beam leaky wave antenna using sinusoidally modulated reactance superposing surface," *IEEE Trans. Antennas Propag.*, vol. 70, no. 12, pp. 12258–12263, Dec. 2022, doi: 10.1109/TAP.2022.3209181.

[13] J. Long, M. M. Jacob, and D. F. Sievenpiper, "Broadband fast-wave propagation in a non-foster circuit loaded waveguide," *IEEE Trans. Microw. Theory Tech.*, vol. 62, no. 4, pp. 789–798, Apr. 2014, doi: 10.1109/TMTT.2014.2309324.

[14] C. K. C. Tzuang and C-C. Lin, "Fast-wave resonance by space-wave leaky mode carrying dominant-mode-like currents," *IEEE Trans. Microw. Theory Tech.*, vol. 46, no. 12, pp. 2444–2449, Dec. 1998, doi: 10.1109/22.739233.

[15] J. Long and D. F. Sievenpiper, "Stable multiple non-Foster circuits loaded waveguide for broadband non-dispersive fast-wave propagation," *Electron. Lett.*, vol. 50, no. 23, pp. 1708–1710, Nov. 2014, doi: 10.1049/el.2014.2612.

[16] H. Jin, Y. Zhou, Y. M. Huang, and K. Wu, "Slow-wave propagation properties of substrate integrated waveguide based on anisotropic artificial material," *IEEE Trans. Antennas Propag.*, vol. 65, no. 9, pp. 4676–4683, Sep. 2017, doi: 10.1109/TAP.2017.2726688.

[17] X. Chen, Z. Li, and J. Wang, "The realizing of radiation null for a SSPPs leaky-wave antenna," in *Proc. IEEE Int. Symp. Microw. Antenna Propag. EMC Technol. MAPE*, 2017, pp. 110–112, doi: 10.1109/MAPE.2017.8250810.

[18] D. Wei, J. Li, J. Yang, Y. Qi, and G. Yang, "Wide-scanning-angle leaky-wave array antenna based on microstrip SSPPs-TL," *IEEE Antennas Wireless Propag. Lett.*, vol. 17, no. 8, pp. 1566–1570, Aug. 2018, doi: 10.1109/LAWP.2018.2855178.

[19] D. Sanchez-Escuderos, M. Ferrando-Bataller, J. I. Herranz, and M. Cabedo-Fabres, "Periodic leaky-wave antenna on planar goubau line at millimeter-wave frequencies," *IEEE Antennas Wireless Propag. Lett.*, vol. 12, pp. 1006–1009, 2013, doi: 10.1109/LAWP.2013.2278035.

[20] Y. L. An, Y. L. Tan, H. B. Zhang, and G. C. Wu, "Double-layered microstrip metamaterial beam scanning leaky wave antenna with consistent gain and low cross-polarization," *Appl. Phys. A*, vol. 123, no. 12, p. 738, 2017, doi: 10.1007/s00339-017-1370-y.

[21] A. Belen, F. Güneş, M. A. Belen, and P. Mahouti, "Microstrip leaky wave antenna for wide range of beam scanning in X band," *Microw. Opt. Technol. Lett.*, vol. 63, no. 10, pp. 2646–2650, 2021, doi: 10.1002/mop.32957.

[22] Y. Chen, K. Wang, Y. Li, and Y. Long, "Periodic microstrip leaky wave antenna with double-sided shorting pins and pairs of slots," *Int. J. Antennas Propag.*, vol. 2020, pp. 1–9, Sep. 2020, doi: 10.1155/2020/7101752.

[23] Z. W. Cheng, H. F. Ma, M. Wang, and T. J. Cui, "Dual-beam leaky-wave radiations with independent controls of amplitude, angle, and polarization based on SSPP waveguide," *Adv. Photon. Res.*, vol. 3, no. 5, 2022, Art. no. 2100313, doi: 10.1002/adpr.202100313.

[24] B. Ren, W. Li, Z. Qin, Y. Wang, L. Zhang, and B. Zhang, "Leaky wave antenna based on periodically truncated SSPP waveguide," *Plasmonics*, vol. 15, no. 2, pp. 551–558, 2020, doi: 10.1007/s11468-019-01081-x.

[25] J. Yi, W. Zhou, Z. Tan, M. Lin, X. Chen, and S. N. Burokur, "Dual-polarized metagrating for controlling diffraction patterns in orthogonal planes," *IEEE Trans. Antennas Propag.*, vol. 71, no. 11, pp. 8753–8761, Nov. 2023, doi: 10.1109/TAP.2023.3315850.

[26] S. Wang et al., "Design and validation of a metagrating for dual-operation," *IEEE Antennas Wireless Propag. Lett.*, vol. 22, pp. 1–5, 2023, doi: 10.1109/LAWP.2023.3308483.

[27] Z. Tan, J. Yi, Q. Cheng, and S. N. Burokur, "Design of perfect absorber based on metagratings: theory and experiment," *IEEE Trans. Antennas Propag.*, vol. 71, no. 2, pp. 1832–1842, Feb. 2023, doi: 10.1109/TAP.2022.3233472.

[28] A. Abolfathi, P. Rezaei, and M. Sharifi, "Compact bilayer substrate integrated waveguide leaky wave antenna with dumbbell-shaped slot based on the TE20 mode," *Int. J. RF Microw. Comput.-Aided Eng.*, vol. 29, no. 8, 2019, Art. no. e21791, doi: 10.1002/mmce.21791.

[29] R. Agrawal, P. Belwal, and S. C. Gupta, "Asymmetric substrate integrated waveguide leaky wave antenna with open stop band suppression and radiation efficiency equalization through broadside," *Radioengineering*, vol. 27, no. 2, pp. 409–416, 2018, doi: 10.13164/re.2018.0409.

[30] R. Agrawal, P. Belwal, M. Singh, and S. C. Gupta, "Continuous beam scanning in substrate integrated waveguide leaky wave antenna," *Prog. Electromagn. Res. M*, vol. 62, pp. 19–28, Nov. 2017, doi: 10.2528/PIERM17091104.

[31] R. Agrawal, P. Belwal, and S. C. Gupta, "Half mode substrate integrated waveguide leaky wave antenna with broadside gain enhancement for ku-band applications," *Radioengineering*, vol. 28, no. 3, pp. 565–571, 2019, doi: 10.13164/re.2019.0565.

[32] L. Ye, Z. Wang, J. Zhuo, F. Han, W. Li, and Q. H. Liu, "A back-fire to forward wide-angle beam steering leaky-wave antenna based on SSPPs," *IEEE Trans. Antennas Propag.*, vol. 70, no. 5, pp. 3237–3247, May 2022, doi: 10.1109/TAP.2021.3137241.

[33] K. Rudramuni et al., "Goubau-line leaky-wave antenna for wide-angle beam scanning from backfire to endfire," *IEEE Antennas Wireless Propag. Lett.*, vol. 17, pp. 1571–1574, 2018, doi: 10.1109/LAWP.2018.2855702.

[34] X. L. Tang et al., "Continuous beam steering through broadside using asymmetrically modulated goubau line leaky-wave antennas," *Sci. Rep.*, vol. 7, Sep. 2017, Art. no. 11685, doi: 10.1038/s41598-017-12118-8.

[35] Y. Pan, Y. Cheng, and Y. Dong, "Surface plasmon polariton leaky-wave antennas with wideband arbitrary multibeam radiation," *IEEE Trans. Antennas Propag.*, vol. 70, no. 2, pp. 931–942, Feb. 2022, doi: 10.1109/TAP.2021.3111210.

[36] J. Chen, W. Yuan, W. X. Tang, L. Wang, Q. Cheng, and T. J. Cui, "Linearly sweeping leaky-wave antenna with high scanning rate," *IEEE Trans. Antennas Propag.*, vol. 69, no. 6, pp. 3214–3223, Jun. 2021, doi: 10.1109/TAP.2020.3037830.

[37] Y. You, Y. Lu, Y. Wang, J. Xu, J. Huang, and W. Hong, "Enhanced pencil-beam scanning CTS leaky-wave antenna based on meander delay line," *IEEE Antennas Wireless. Propag. Lett.*, vol. 20, no. 9, pp. 1760–1764, Sep. 2021, doi: 10.1109/LAWP.2021.3096084.

[38] H. Jiang et al., "Backward-to-forward wide-angle fast beam-scanning leaky-wave antenna with consistent gain," *IEEE Trans. Antennas Propag.*, vol. 69, no. 5, pp. 2987–2992, May 2021, doi: 10.1109/TAP.2020.3029721.

[39] J. Zhong, A. K. Rashid, and Q. Zhang, "45 & x00B0; linearly polarized and circularly polarized high-scanning-rate leaky-wave antennas based on slotted substrate integrated waveguide," *IEEE Access*, vol. 8, pp. 82162–82172, 2020, doi: 10.1109/ACCESS.2020.2991180.

[40] G. Zhang, Q. Zhang, S. Ge, Y. Chen, and R. Murch, "High scanning-rate leaky-wave antenna using complementary microstrip-slot stubs," *IEEE Trans. Antennas Propag.*, vol. 67, no. 5, pp. 2913–2922, May 2019, doi: 10.1109/TAP.2019.2896704.

[41] E. Abdo-Sanchez, A. Epstein, and G. V. Eleftheriades, "Reconfigurability mechanisms with scanning rate control for omega-bianisotropic huygens' metasurface leaky-wave antennas," *IEEE Access*, vol. 7, pp. 168247–168260, 2019, doi: 10.1109/ACCESS.2019.2953779.

[42] D.-F. Guan, Q. Zhang, P. You, Z.-B. Yang, Y. Zhou, and S.-W. Yong, "Scanning rate enhancement of leaky-wave antennas using slow-wave substrate integrated waveguide structure," *IEEE Trans. Antennas Propag.*, vol. 66, no. 7, pp. 3747–3751, Jul. 2018, doi: 10.1109/TAP.2018.2831257.

[43] G. Zhang, Q. Zhang, Y. Chen, and R. Murch, "High scanning rate circularly polarized leaky-wave antennas based on allpass filtering network," in *Proc. IEEE Asia-Pacific Microw. Conf. (APMC)*, 2019, pp. 1026–1028. doi: 10.1109/APMC46564.2019.9038654.

[44] *Copper Foils for High Frequency Materials*, Rogers Corp., Chandler, Arizona, USA, 2021.

[45] Y. Han, J. Wang, S. Gong, Y. Li, Y. Zhang, and J. Zhang, "Low RCS antennas based on dispersion engineering of spoof surface plasmon polaritons," *IEEE Trans. Antennas Propag.*, vol. 66, no. 12, pp. 7111–7116, Dec. 2018, doi: 10.1109/TAP.2018.2869206.

[46] S.-D. Xu et al., "A wide-angle narrowband leaky-wave antenna based on substrate integrated waveguide-spoof surface plasmon polariton structure," *IEEE Antennas Wireless. Propag. Lett.*, vol. 18, pp. 1386–1389, 2019, doi: 10.1109/LAWP.2019.2917561.

YUE WANG received the B.S. degree in electromagnetic fields and wireless technology and the M.S. degree in electromagnetic fields and microwave technology from the Harbin Institute of Technology, Harbin, China, in 2018, and 2020, respectively, where he is currently pursuing the Ph.D. degree in electronic science and technology with the School of Astronautics.

SHENGYING LIU received the B.S. degree in communication engineering and the M.S. degree in electromagnetic fields and microwave technology from the Harbin Institute of Technology, Harbin, China, in 2011 and 2013, respectively, where he is currently pursuing the Ph.D. degree with the School of Electronic and Information Engineering. Since 2013, he has been with the Department of Antenna, Beijing Institute of Remote Sensing Equipment, Beijing, China, where he is currently an Engineer. His current research interests include the phased array antenna technology: phased array beam forming theory, design of antenna elements, and T/R module integrated technology; and the continuous transverse stub array.

CHUNSHENG GUAN was born in Henan, China, in 1994. He received the B.S. degree in electromagnetic fields and wireless technology from the Harbin Institute of Technology, weihai, China, in 2017, and the Ph.D. degree in communication and information systems from the Harbin Institute of Technology, Harbin, China, in 2022. He has been with the Air Force Engineering University, where he is currently a Lecturer. His current research interests include metasurface-based devices and antennas.

HAO YU received the B.S. and M.S. degrees in electromagnetic field and microwave technology from the Harbin Institute of Technology, Harbin, China, in 2010 and 2014, respectively. He is currently an Engineer with the Beijing Institute of Electronic System Engineering. His research interests are in the areas of metasurface and electromagnetic pulse protection.

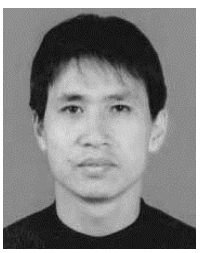

JINXIANG WANG received the B.S. and M.S. degrees in semiconductor physics and the Ph.D. degree in communication and information engineering from the Harbin Institute of Technology, Harbin, China, in 1990, 1993, and 1999, respectively, where he is currently a Professor with Microelectronics Center. His research interests are very-large-scale integration design, wireless communication, system on chip, and network on chip.

QUN WU (Senior Member, IEEE) received the B.Sc. degree in radio engineering, the M.Eng. degree in electromagnetic fields and microwave technology, and the Ph.D. degree in communication and information systems engineering from the Harbin Institute of Technology, Harbin, China, in 1977, 1988, and 1999, respectively. From 1998 to 1999, he was a Visiting Professor with Seoul National University, Seoul, South Korea. From 1999 to 2000, he was a Visiting Professor with the Pohang University of Science and Technology, Pohang, South Korea. Since 1990, he has been with the Department of Electronic and Communication Engineering, Harbin Institute of Technology, where he is currently a Professor. He has authored or coauthored over 50 international and regional refereed journal articles. His recent research interests include microwave active circuits, electromagnetic compatibility, monolithic microwave integrated circuits, and millimeter-wave micro electromechanical systems devices. He was a recipient of two third-class prizes and one second-class prize of Scientific Progress Awards from the Ministry of Aerospace of China in 1989 and 1992, respectively.

CHANGFEI ZHOU received the B.S. and M.S. degrees in communication engineering from the Harbin Institute of Technology, Harbin, China, in 2012 and 2014, and the Ph.D. degree from the University of Hong Kong, Hong Kong, China, in 2018. From 2018 to 2019, he was an Antenna Engineer with LSCM Research Centre, Hong Kong. Since 2019, he has been a lecture with the Dalian University of Technology. His current research interests include multiband and wideband antennas, RFID, and metasurface design.

XUMIN DING (Member, IEEE) received the B.S. degree in communication engineering, the M.S. degree in electromagnetic fields and microwave technology, and the Ph.D. degree in microelectronics and solid state electronics from the Harbin Institute of Technology, Harbin, China, in 2010, 2012, and 2015, respectively. He has been with the Harbin Institute of Technology, where he is currently a Professor.